doi:10.1093/brain/awy059 BRAIN 2018: 141; 1517–1528 | 1517

BRAIN
A JOURNAL OF NEUROLOGY

Longitudinal tau PET in ageing and Alzheimer's disease

Clifford R. Jack, Jr,[1] Heather J. Wiste,[2] Christopher G. Schwarz,[1] Val J. Lowe,[3] Matthew L. Senjem,[4] Prashanthi Vemuri,[1] Stephen D. Weigand,[2] Terry M. Therneau,[2] Dave S. Knopman,[5] Jeffrey L. Gunter,[4] David T. Jones,[5] Jonathan Graff-Radford,[5] Kejal Kantarci,[1] Rosebud O. Roberts,[2,5] Michelle M. Mielke,[2] Mary M. Machulda[6] and Ronald C. Petersen[2,5]

See Hansson and Mormino (doi:10.1093/brain/awy065) for a scientific commentary on this article.

Our objective was to compare different whole-brain and region-specific measurements of within-person change on serial tau PET and evaluate its utility for clinical trials. We studied 126 individuals: 59 cognitively unimpaired with normal amyloid, 37 cognitively unimpaired with abnormal amyloid, and 30 cognitively impaired with an amnestic phenotype and abnormal amyloid. All had baseline amyloid PET and two tau PET, MRI, and clinical assessments. We compared the topography across all cortical regions of interest of tau PET accumulation rates and the rates of four different whole-brain or region-specific meta-regions of interest among the three clinical groups. We computed sample size estimates for change in tau PET, cortical volume, and memory/mental status indices for use as outcome measures in clinical trials. The cognitively unimpaired normal amyloid group had no observable tau accumulation throughout the brain. Tau accumulation rates in cognitively unimpaired abnormal amyloid were low [0.006 standardized uptake value ratio (SUVR), 0.5%, per year] but greater than rates in the cognitively unimpaired normal amyloid group in the basal and mid-temporal, retrosplenial, posterior cingulate, and entorhinal regions of interest. Thus, the earliest elevation in accumulation rates was widespread and not confined to the entorhinal cortex. Tau accumulation rates in the cognitively impaired abnormal amyloid group were 0.053 SUVR (3%) per year and greater than rates in cognitively unimpaired abnormal amyloid in all cortical areas except medial temporal. Rates of accumulation in the four meta-regions of interest differed but only slightly from one another. Among all tau PET meta-regions of interest, sample size estimates were smallest for a temporal lobe composite within cognitively unimpaired abnormal amyloid and for the late Alzheimer's disease meta-region of interest within cognitively impaired abnormal amyloid. The ordering of the sample size estimates by outcome measure was MRI < tau PET < cognitive measures. At a group-wise level, observable rates of short-term serial tau accumulation were only seen in the presence of abnormal amyloid. As disease progressed to clinically symptomatic stages (cognitively impaired abnormal amyloid), observable rates of tau accumulation were seen uniformly throughout the brain providing evidence that tau does not accumulate in one area at a time or in start-stop, stepwise sequence. The information captured by rate measures in different meta-regions of interest, even those with little topographic overlap, was similar. The implication is that rate measurements from simple meta-regions of interest, without the need for Braak-like staging, may be sufficient to capture progressive within-person accumulation of pathologic tau. Tau PET SUVR measures should be an efficient outcome measure in disease-modifying clinical trials.

1 Department of Radiology, Mayo Clinic, 200 First Street SW, Rochester, MN 55905, USA
2 Department of Health Sciences Research, Mayo Clinic, 200 First Street SW, Rochester, MN 55905, USA
3 Department of Nuclear Medicine, Mayo Clinic, 200 First Street SW, Rochester, MN 55905, USA
4 Department of Information Technology, Mayo Clinic, 200 First Street SW, Rochester, MN 55905, USA
5 Department of Neurology, Mayo Clinic, 200 First Street SW, Rochester, MN 55905, USA
6 Department of Psychiatry and Psychology, Mayo Clinic, 200 First Street SW, Rochester, MN 55905, USA

Received November 27, 2017. Revised January 8, 2018. Accepted January 14, 2018. Advance Access publication March 12, 2018

Correspondence to: Clifford R. Jack, Jr
200 First St. SW
Rochester, MN 55905, USA
E-mail: Jack.clifford@mayo.edu

Keywords: tau PET; brain ageing; Alzheimer's disease; Alzheimer's biomarkers; amyloid PET

Abbreviations: CI/U A+/− = cognitively impaired/unimpaired individuals with/without abnormal amyloid PET; MCI = mild cognitive impairment; PVC = partial volume correction; SUVR = standardized uptake value ratio

Introduction

A number of studies have described the characteristics of cross-sectional tau PET imaging in ageing and Alzheimer's disease (Villemagne *et al.*, 2015; Brier *et al.*, 2016; Chhatwal *et al.*, 2016; Cho *et al.*, 2016; Gordon *et al.*, 2016; Johnson *et al.*, 2016; Ossenkoppele *et al.*, 2016; Scholl *et al.*, 2016; Schwarz *et al.*, 2016; Wang *et al.*, 2016; Bejanin *et al.*, 2017; Buckley *et al.*, 2017; Jones *et al.*, 2017; La Joie *et al.*, 2017; Marks *et al.*, 2017; Nasrallah *et al.*, 2018; Sepulcre *et al.*, 2017; Lowe *et al.*, 2018; Phillips *et al.*, 2018). Few, however, have addressed longitudinal tau PET (Chiotis *et al.*, 2017; Southekal *et al.*, 2017). Because within-person changes in Alzheimer's disease biomarkers over short time periods are typically small in magnitude (Fox *et al.*, 2000), close attention to methods of measurement should be important for effectively capturing within-person change on tau PET. One key methodological question is: where in the brain should measures be taken to best capture rates of accumulation of pathological tau in ageing and Alzheimer's disease?

Our main objective was to compare within-person change on serial tau PET across various cortical regions. To address different stages of the typical Alzheimer's continuum, we studied three groups of participants: cognitively unimpaired individuals with normal amyloid PET (CU A−, i.e. individuals not in the Alzheimer's continuum); cognitively unimpaired individuals with abnormal amyloid PET (CU A+, i.e. individuals who were early in the Alzheimer's continuum), and cognitively impaired (amnestic phenotype) individuals with abnormal amyloid PET (CI A+).

We had four aims: (i) to examine and compare the topography of tau PET accumulation rates across all cortical regions of interest among the three clinical groups; (ii) to identify meta-regions of interest that optimally captured change early in the Alzheimer's continuum, and later in the Alzheimer's continuum; (iii) to compare the characteristics of longitudinal tau PET among the three clinical groups using four different meta-regions of interest: the early and the late Alzheimer's disease change regions of interest, the whole brain, and a previously reported temporal meta-region of interest (Jack *et al.*, 2017); and (iv) to compare sample size estimates for change in tau PET, cortical volume and memory/mental status indices for use as outcome measures in clinical trials.

Materials and methods

Participant recruitment, characterization and inclusion criteria

All individuals in this study were participants enrolled in one of two studies. The Mayo Clinic Study of Aging (MCSA) is a population-based study of cognitive ageing among Olmsted County, Minnesota residents (Roberts *et al.*, 2008). All individuals without a medical contraindication are invited to participate in imaging studies. The Mayo Alzheimer's Disease Research Center (ADRC) is a longitudinal research study of individuals recruited from clinical practice. Both studies were approved by the Mayo Clinic and Olmsted Medical Center Institutional Review Boards and written informed consent was obtained from all participants.

Evaluations included a medical history review and interview with a study partner performed by a study coordinator; a medical history review, mental status examination, and a neurological examination by a physician; and a neuropsychological examination (Roberts *et al.*, 2008). Participants were assigned a diagnosis of cognitively unimpaired [CU, defined as not mild cognitive impairment (MCI) or dementia], MCI (Petersen, 2004) or demented (McKhann *et al.*, 2011) using established criteria. MCI and demented individuals were combined into a single cognitively impaired (CI) group. Memory performance was assessed in cognitively unimpaired individuals by a composite from the following: the Wechsler Memory Scale-Revised (WMS-R) Logical Memory-II (delayed recall), WMS-R Visual Reproduction-II (delayed recall), and the Auditory Verbal Learning Test (delayed recall). Mental status was assessed among cognitively impaired participants by the Short Test of Metal Status (Kokmen *et al.*, 1991).

All cognitively impaired participants were required to have abnormal amyloid (A+) based on amyloid PET criteria published previously (Jack *et al.*, 2017). This was done to create a biologically homogeneous group of cognitively impaired individuals who were in the Alzheimer's continuum. All cognitively impaired participants were also required to have an amnestic clinical presentation. Because the topographic distribution of pathologic tau correlates closely with clinical presentation (Ossenkoppele *et al.*, 2016; Jones *et al.*, 2017; Xia *et al.*, 2017; Phillips *et al.*, 2018), requiring an amnestic clinical presentation created a group of impaired individuals with a fairly homogenous tau PET 'phenotype'. Our groups of participants were selected with the idea that contrasts between CU A+ versus CU A− would reveal areas of the brain that capture change in tau PET seen early in the Alzheimer's

continuum. Contrasts between CI A+ versus CU A+ would reveal areas of the brain that capture change in tau PET seen later in the Alzheimer's continuum.

All MCSA and ADRC participants who met the clinical criteria above and had two imaging assessments, which in our protocol includes amyloid PET, tau PET and MRI, were included in this study. Imaging assessments were ~12–15 months apart and were performed between 20 April 2015 and 29 August 2017.

PET

Amyloid PET imaging was performed with Pittsburgh compound B (Klunk *et al.*, 2004). Tau PET was performed with AV1451, synthesized on site with precursor supplied by Avid Radiopharmaceuticals (Schwarz *et al.*, 2016). Late uptake amyloid PET images were acquired 40–60 min and tau PET 80–100 min after injection. CT was obtained for attenuation correction.

Amyloid PET and tau PET were analysed with our in-house fully automated image processing pipeline where image voxel values are extracted from automatically labelled regions of interest propagated from an MRI template. Amyloid and tau PET standardized uptake value ratio (SUVR) values were formed by normalizing target regions of interest to the cerebellar crus grey matter (Jack *et al.*, 2017). The amyloid PET target was the prefrontal, orbitofrontal, parietal, temporal, anterior cingulate, posterior cingulate and precuneus regions of interest (Jack *et al.*, 2017). Amyloid PET data were not partial volume corrected. The cut-point used to define abnormality (i.e. A+) on amyloid PET was SUVR 1.42 [centiloid 19 (Klunk *et al.*, 2015)] based on the threshold value beyond which the rate of change in amyloid PET reliably increases (Jack *et al.*, 2017).

Tau PET data were processed as follows: following PET to magnetic resonance spatial registration, a binary brain tissue mask (from the MRI) was resampled into PET voxel dimensions and smoothed with a 6 mm full-width at half-maximum Gaussian filter (approximately the point spread function of the PET camera) to generate a smoothed tissue mask. At each voxel the PET image was divided by the value in the mask to generate a partial volume corrected (PVC) PET image (Meltzer *et al.*, 1990). An unsmoothed binary MRI grey matter mask was then applied to the PVC PET image to give a grey matter sharpened PET image. Atlas region of interest values were extracted as above for amyloid PET. For comparison, we also analysed PET images without PVC.

MRI

MRI was performed on one of three 3-T systems from the same vendor (General Electric). Longitudinal change in cortical volume was measured using a previously described algorithm developed in-house called TBM-SyN (described in detail in Vemuri *et al.*, 2015). TBM-SyN is one of the data analysis types provided by the Alzheimer's Disease Neuroimaging Initiative (http://adni.loni.usc.edu/).

Statistical methods

Annual change in tau PET for each individual and each region of interest was calculated as the difference in tau PET SUVR between the two scans divided by time between scans. Linear regression models with these annual change values as the outcome (y) and clinical group as the predictor (x) were used to estimate mean differences in rates of tau PET accumulation across the three clinical groups for individual regions of interest and the four meta-regions of interest. The four meta-regions of interest evaluated were: (i) an early Alzheimer's disease change composite; (ii) a late Alzheimer's disease change composite; (iii) the whole brain; and (iv) a temporal composite.

For defining the early and late Alzheimer's disease change meta-regions of interest, we used penalized logistic regression models to identify a parsimonious set of regions that optimized separation between CU A− and CU A+ (i.e. early changes) and between CU A+ and CI A+ (i.e. later changes). The penalty in these models was an elastic net, which penalizes both the sum of squares of the regression coefficients (i.e. a 'ridge' penalty) and the sum of absolute values of the coefficients (i.e. a 'lasso' penalty). We used weights of 0.8 for the lasso portion of the penalty and 0.2 for the ridge portion (Hasite *et al.*, 2009). Varying this penalty from nothing (i.e. no shrinkage of the regression coefficients and all regions of interest in the model) to a full penalty in which all regression coefficients are shrunk to zero (i.e. an intercept only model with no regions of interest), we used cross-validation to identify the optimal model. We took the average of the tau PET SUVR values across the regions identified by the early Alzheimer's disease rate model, to form the early Alzheimer's disease change meta-region of interest. Similarly, we took the average of the tau PET SUVR values across regions identified by the late Alzheimer's disease rate model, to form the late Alzheimer's disease change meta-region of interest. The regions included in the early and late Alzheimer's disease change meta-regions of interest are described in the results.

The whole brain meta-region of interest was defined as the voxel-number weighted average of tau PET SUVR in all 41 allo- and iso-cortical regions of interest. The temporal composite, defined in an earlier study to separate CU A− and CI A+ groups cross-sectionally (membership partially overlapped with individuals in the present study) (Jack *et al.*, 2017), was calculated as the voxel-number weighted average of tau PET SUVR in the entorhinal cortex, amygdala, parahippocampal, fusiform, inferior temporal, and middle temporal regions of interest.

We used Spearman rank correlations among all participants between pairs of the four meta-regions of interest to assess similarities in the measurements.

We calculated sample size estimates per arm for a hypothetical clinical trial designed to have 80% power to detect a 25% reduction in annual change in each marker with two-sided alpha of 0.05. Given these parameters, the sample size is proportional to the square of standard deviation (SD)/mean where the inverse of this quantity, mean/SD, is the estimated effect size. The uncertainty of this effect size estimate (mean/SD) was summarized using the SD of 10 000 bootstrap replicates. We calculated effect sizes and corresponding sample size estimates within CU A+ and CI A+ groups for the four tau PET meta-regions of interest, for an anatomic MRI-based biomarker (TBM-SyN, cortical volume), and for a cognition measure. Because floor/ceiling effects differ between cognitively unimpaired and impaired individuals, cognition was assessed with a memory composite among CU A+ and with the Short Test of Mental Status among CI A+.

Table 1 Demographic characteristics of participants at baseline

Characteristic	All	CU A−	CU A+	CI A+[a]
Number of subjects	126	59	37	30
Study, *n* (%)				
MCSA	96 (76)	57 (97)	33 (89)	6 (20)
ADRC	30 (24)	2 (3)	4 (11)	24 (80)
Age, years				
Median (IQR)	73 (64, 80)	66 (58, 74)	80 (75, 85)	74 (71, 77)
Range	52–94	52–94	58–94	59–94
Sex, *n* (%)				
Female	52 (41)	24 (41)	19 (51)	9 (30)
Male	74 (59)	35 (59)	18 (49)	21 (70)
Education, years				
Median (IQR)	16 (13, 17)	16 (14, 18)	14 (13, 17)	16 (13, 17)
Range	7–20	12–20	8–18	7–20
APOE ε4, *n* (%)				
Non-carrier	66 (53)	43 (73)	17 (46)	6 (21)
Carrier	59 (47)	16 (27)	20 (54)	23 (79)
Amyloid PET, SUVR				
Median (IQR)	1.45 (1.32, 2.11)	1.31 (1.26, 1.35)	1.68 (1.51, 2.11)	2.43 (2.11, 2.77)
Range	1.15–3.34	1.15–1.40	1.42–2.84	1.50–3.34
Scan interval, years				
Median (IQR)	1.2 (1.1, 1.4)	1.3 (1.1, 1.4)	1.3 (1.2, 1.3)	1.1 (1.0, 1.1)
Range	0.8–2.2	1.0–1.6	1.1–2.0	0.8–2.2

[a]The CI A+ group includes 11 (37%) individuals with MCI and 19 (63%) individuals with multi-domain amnestic dementia.

Results

Characteristics of participants

Nearly all (94%) cognitively unimpaired individuals were participants in the MCSA while most (80%) cognitively impaired individuals were participants in the ADRC (Table 1). About two-thirds of the CI A+ individuals carried a diagnosis of amnestic multi-domain dementia and one-third a diagnosis of amnestic MCI (i.e. prodromal Alzheimer's disease). CU A− was the youngest group and CU A+ the oldest. The sex distribution was roughly even in the cognitively unimpaired groups while the CI A+ group had more males. The proportion of *APOE* 4 carriers increased progressively from CU A− to CU A+ to CI A+. The median time interval between serial imaging sessions was 1.3 years for the cognitively unimpaired groups and 1.1 years for CI A+.

Rates by region of interest and clinical group

On average, the tau PET accumulation rate was near zero in the CU A− group in all regions of interest (Fig. 1). Rates of tau accumulation in CU A+ were generally low (0.006 SUVR, 0.5%, per year) but were greater than the rates in CU A− in the entorhinal, fusiform, inferior and mid-temporal, temporal pole, retrosplenial, and the posterior cingulate regions of interest. The CI A+ group had rates of tau accumulation around 0.053 SUVR (3%) per year, which was higher than the rates in the CU A+ group in all regions of interest except the medial temporal regions of entorhinal cortex and amygdala (Fig. 1). Because of small numbers in both MCI and dementia groups, dementia and MCI were combined into a CI A+ group for the main analysis (as was done in the PRIME trial) (Sevigny *et al.*, 2016). Supplementary Fig. 1 shows that while rates were generally higher in dementia than MCI, many of these differences were not significant. The general pattern of the CU A+ versus MCI and CU A+ versus dementia contrasts shared similar features including pronounced differences from CU A+ in the basal and mid-temporal and occipital regions of interest.

We found a positive association between tau change and age in the CU A− group; however, this was not seen consistently across all regions of interest. Of 32 regions of interest, the median rank correlation was +0.18 [interquartile range (IQR) +0.13 to +0.24]. On the other hand, in the CU A+ group there was no evidence of an association between accumulation rate and age. The median rank correlation was 0 (IQR −0.06 to +0.09). The CI A+ group tended to have negative associations between rate of change and age with a median correlation of −0.21 (IQR −0.31 to −0.18); however, this was not seen consistently across all regions of interest.

Selecting meta-regions of interest that most robustly capture early and later Alzheimer's disease change

From the logistic penalized regression model, the regions of interest that best separated CU A+ and CU A− were the fusiform and posterior cingulate gyrus (Supplementary

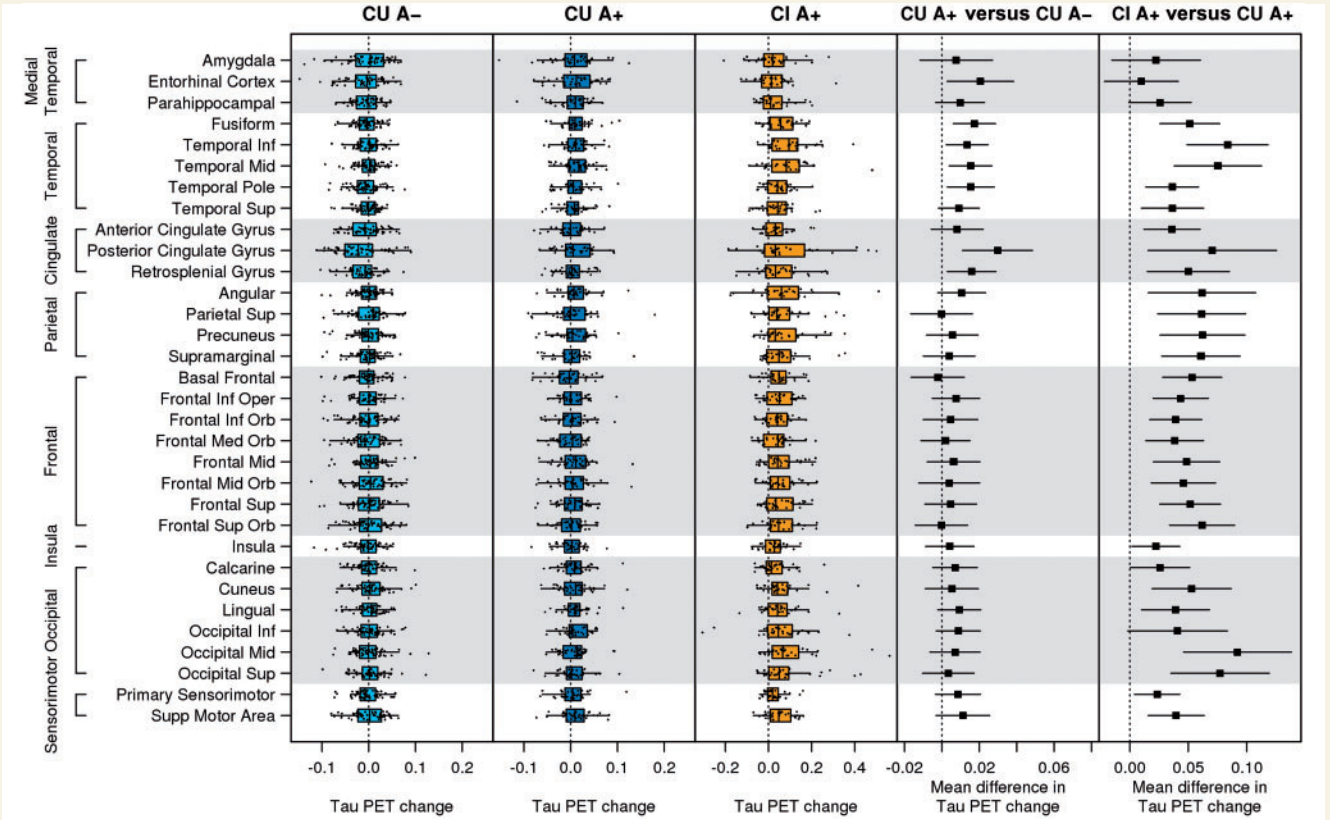

Figure 1 Regional annual change in tau PET by group. Box plots of annual change in regional tau PET (SUVR per year) among CU A–, CU A+, and CI A+ are shown in the first three panels. Estimated mean difference [95% confidence interval (CI)] in annual change in regional tau PET (SUVR per year) between CU A– versus CU A+ and CU A+ versus CI A+ are shown in the last two columns. A reference line is shown at 0. Note that the range of the *x*-axis scale is wider for CI A+ than CU A+ or CU A–.

Fig. 2). We refer to this as the early Alzheimer's disease change meta-region of interest. The regions of interest that best separated CI A+ and CU A+ (Supplementary Fig. 2) were the inferior temporal, superior orbital frontal, basal frontal (olfactory and gyrus rectus), and middle occipital. We refer to this as the late Alzheimer's disease change meta-region of interest.

Comparison of four meta-region of interest rate measures

We compared group-wise rates of tau accumulation for the early and late Alzheimer's disease change meta-regions of interest and the whole brain and temporal composite meta-regions of interest. The mean difference in tau accumulation between CI A+ and CU A+ was 0.061, 0.073, 0.046, and 0.062 SUVR per year for the early Alzheimer's disease, late Alzheimer's disease, whole brain, and temporal composite meta-regions of interest, respectively ($P \leqslant 0.001$ for all) (Fig. 2). The late Alzheimer's disease and whole brain meta-regions of interest did not separate CU A+ from CU A– [0.004 SUVR difference ($P = 0.42$) and 0.008 SUVR difference ($P = 0.14$) per year]. However, tau accumulation rates were greater in CU A+ than CU A– for the early Alzheimer's disease and temporal composite meta-regions of interest, 0.024 ($P < 0.001$) and 0.015 ($P = 0.005$) SUVR per year, respectively.

Pairwise scatter plots of annual change in tau PET SUVR for the four meta-regions of interest are shown in Supplementary Fig. 3. The late Alzheimer's disease change, whole brain, and temporal composite meta-regions of interest were all highly correlated with each other (Spearman rank correlation varied from 0.87 to 0.93). Correlations between the early Alzheimer's disease change and each of the other three meta-regions of interest were slightly more modest (0.73 to 0.82).

Trajectory plots (Fig. 3) show the SUVR at each time point for each individual for the four meta-regions of interest. The rate patterns of individual participants by age and clinical group are similar for all four meta-regions of interest.

Sample size estimates

We estimated sample sizes per arm that would be needed to power a clinical trial using a conservative 25% therapeutic reduction in the natural rate of change as an outcome measure. For a trial in CU A+ individuals, the smallest sample size among the four tau PET meta-regions of

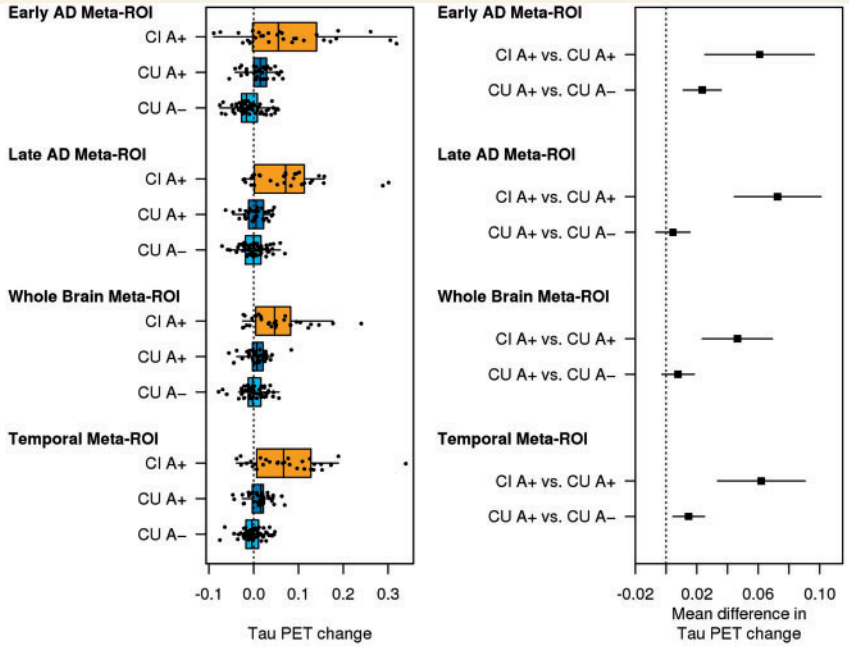

Figure 2 Annual change in tau PET by group for four meta-regions of interest. Box plots of annual change in tau PET (SUVR per year) by clinical group for the four different meta-regions of interest (*left*). Estimated mean difference (95% CI) in annual change in tau PET (SUVR per year) between CI A+ versus CU A+ and CU A+ versus CU A– from linear regression models (*right*). A reference line is shown at 0. ROI = region of interest.

interest was the temporal meta-region of interest ($n = 1087$, Table 2). TBM-SyN sample size was the smallest ($n = 455$) and the memory composite was the largest ($n = 1360$). For a trial in CI A+, the smallest sample size among the tau meta-regions of interest was the late meta-region of interest ($n = 282$). TBM-SyN sample size was again the smallest ($n = 212$) and the mental status exam was the largest ($n = 623$).

For comparison purposes tau PET sample sizes with and without PVC are shown in Table 3. These data show that mean rates of change and variance are generally greater, and sample size estimates are smaller with PVC than without in the CU A+ and CI A+ groups for all four meta-regions of interest with one exception.

Discussion

In this longitudinal analysis of tau PET we found short-term serial SUVR measurements provided meaningful information about accumulation rates of pathological tau. Our first aim was to examine and compare the regional topography of tau accumulation rates among the different clinical groups across all cortical regions of interest. Early in the disease (CU A+), rates of accumulation were elevated relative to CU A– in the basal and mid-temporal and limbic areas, while later in the disease (CI A+) rates were elevated relative to CU A+ in all areas of the cortex except the medial temporal lobe (Fig. 1). These results are somewhat consistent with the Braak and Braak (1991) model of regional expansion of pathological tau in Alzheimer's disease in that an increased rate of accumulation of pathological tau appeared earlier in the disease process in the medial temporal lobe than in most neocortical areas. However, that fact that elevated rates in CU A+ relative to CU A– were not confined to the entorhinal cortex suggests that early tau accumulation may not be as spatially restricted as implied in Braak staging (Braak and Braak, 1991).

We also found that entorhinal cortex and amygdala accumulation rates were not different between CI A+ and CU A+ (Fig. 1). This suggests that as the disease progresses, pathological tau accumulation continues in areas involved earlier (which is a feature of the Braak and Braak model) (Braak and Braak, 1997). That is, it is not the case that pathological tau accumulates in an early Braak location, during which time higher Braak areas are uninvolved, and then accumulation moves to the next higher Braak area, during which time tau is no longer accumulating in earlier areas. Our findings do not conflict with the concept of prion-like spread of tau (de Calignon *et al.*, 2012; Liu *et al.*, 2012), but do conflict with the idea that increases in total brain tau burden are attributable only to spread of tau from one uninvolved area to the next. These data suggest that rather than measure progression as change from lower to higher Braak stages, progression can be measured effectively as increasing burden within a single combination of tau PET regions of interest. Thus, quantification of change in tau PET can be accomplished in the same manner as is commonly done in other modalities—i.e. amyloid and FDG PET, and MRI.

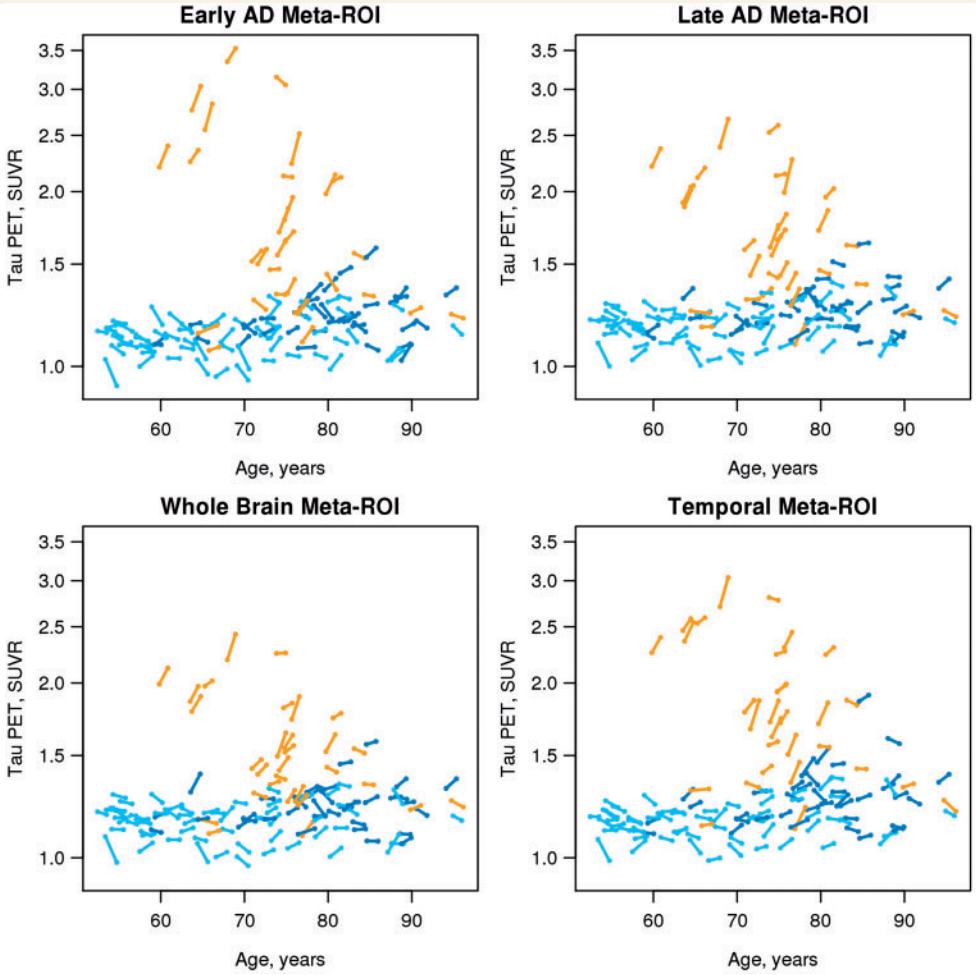

Figure 3 Individual tau PET trajectory plots by age, group and meta-region of interest. Individual trajectory plots showing tau PET by age for all individuals for the four different meta-region of interest definitions. Colours represent clinical group: CU A− = light blue; CU A+ = dark blue; CI A+ = gold; ROI = region of interest.

At a group-wise level, observable rates of short-term serial tau accumulation were only seen in the presence of abnormal amyloid (i.e. CU A+ and CI A+). This supports the idea that amyloidosis is an upstream driver of tau accumulation (Jack *et al.*, 2013; Pontecorvo *et al.*, 2017). We did find that rates of tau accumulation were positively associated with age among CU A− subjects in some regions of interest, and negatively associated with age among CI A+ in some regions of interest. However, neither of these associations was consistently present across anatomically contiguous regions of interest and therefore we did not age-adjust our intergroup rate comparisons.

Our second aim was to select meta-regions of interest that most robustly capture early and later change in subjects who are in the Alzheimer's continuum. This was accomplished with our CU A− versus CU A+ and CU A+ versus CI A+ penalized logistic regression models. We emphasize that the individual regions of interest selected in the penalized regression models were not the only ones that changed early and later, respectively, but simply a parsimonious set of regions of interest that independently discriminated between groups (Supplementary Fig. 2). Our early Alzheimer's disease change meta-region of interest included the posterior cingulate and fusiform regions. Although the entorhinal cortex rate was greater in CU A+ than CU A−, it was not identified as one of the regions included in our early Alzheimer's disease change meta-region of interest. This suggests that pathological tau appears early in limbic and neocortical temporal lobe areas in addition to the entorhinal cortex, which is not generally considered to be the case in the Braak model of tau progression. The more widespread tau accumulation may not have been appreciated in autopsy studies because areas like the posterior cingulate are not traditionally included in standard autopsy blocks. Regions selected for the late Alzheimer's disease change meta-region of interest do fit the traditional notions of Braak and Braak staging in that the late Alzheimer's disease change regions of interest were all located outside medial temporal areas.

Table 2 Sample size estimates

Parameter	CU A+			CI A+		
	Change/year Mean (SD)	Effect size (SE)[a]	*n*	Change/year Mean (SD)	Effect size (SE)[a]	*n*
Tau PET						
Early AD meta-ROI	0.013 (0.028)	0.45 (0.19)	1228	0.074 (0.104)	0.71 (0.16)	499
Late AD meta-ROI	0.004 (0.025)	0.17 (0.18)	8805	0.077 (0.081)	0.95 (0.17)	282
Whole brain meta-ROI	0.007 (0.025)	0.27 (0.18)	3513	0.053 (0.064)	0.83 (0.16)	364
Temporal meta-ROI	0.012 (0.026)	0.48 (0.19)	1087	0.074 (0.082)	0.91 (0.18)	308
TBM-SyN	−0.8 (1.1)	−0.74 (0.17)	455	−2.2 (2.0)	−1.09 (0.19)	212
Cognition[b]	−0.17 (0.40)	−0.43 (0.20)	1360	−2.4 (3.8)	−0.64 (0.19)	623

Sample size estimates per arm for a clinical trial targeting a 25% reduction in annual change in a marker with 80% power and alpha = 0.05 within CU A+ and CI A+.
[a]Effect size is calculated as the mean divided by the standard deviation in the sample. The standard error of the effect size is determined from 10 000 bootstrap replicates.
[b]Cognition is measured as annual change in memory composite z-score among CU A+ and as annual change in Short Test of Mental Status among CI A+.
AD = Alzheimer's disease; ROI = region of interest.

Our third aim was to compare the characteristics of longitudinal tau PET among the three clinical groups using four different meta-regions of interest. Varying opinions exist about how to measure tau burden cross-sectionally (Maass *et al.*, 2017). Some advocate using a Braak-like staging approach (Cho *et al.*, 2016; Scholl *et al.*, 2016; Schwarz *et al.*, 2016). Others suggest that abnormal tau uptake tends to be widely distributed rather than deposited focally in a stepwise and sequential manner (Brier *et al.*, 2016; Gordon *et al.*, 2016; Jones *et al.*, 2017; Mishra *et al.*, 2017; Lowe *et al.*, 2018). Our data indicate that the information on rates of tau accumulation captured by different meta-regions of interest, while not identical, is quite similar. Pairwise scatter plots among the four rate measures (Supplementary Fig. 3) reveal that the late Alzheimer's disease change, whole brain, and temporal composite meta-regions of interest all correlate extremely well with each other and although each correlates slightly less well with the early Alzheimer's disease change meta-region of interest, correlations between the early Alzheimer's disease change meta-region of interest and the others are still high. Similarly, Fig. 3 demonstrates that the four different tau PET meta-regions of interest capture similar relationships between age, clinical group and tau accumulation trajectories in individual subjects. The implication is that change measurements from simple meta-regions of interest, without the need for Braak-like staging, may be sufficient to capture progressive within-person accumulation of pathological tau. In particular we draw attention to the fact that the late Alzheimer's disease change meta-region of interest and the temporal composite have little topographic overlap (only the inferior temporal region), likewise the early Alzheimer's disease change meta-region of interest and the temporal composite have only the fusiform gyrus in common (Fig. 4), yet the age, clinical group and individual tau accumulation trajectory patterns are extremely similar.

While cross-sectional results were not the focus of this paper, Fig. 3 illustrates that baseline values are generally greater among younger versus older CI A+ individuals for all four meta-regions of interest. In particular, under age 70 there is a noticeable separation between the tau PET SUVR values in most cognitively impaired individuals and the SUVR values in the cognitively unimpaired individuals. However, at older ages, there is more overlap in the SUVR values across the cognitively impaired and unimpaired groups. The phenomenon of greater cross-sectional tau PET binding in early onset versus late onset sporadic Alzheimer's disease has been described (Ossenkoppele *et al.*, 2016; Koychev *et al.*, 2017; Scholl *et al.*, 2017; Lowe *et al.*, 2018). Our interpretation of this phenomenon is that older individuals with symptomatic Alzheimer's disease are more likely to have comorbid non-Alzheimer's disease brain pathological change (Markesbery *et al.*, 2006; Schneider *et al.*, 2009; Nelson *et al.*, 2011; Sonnen *et al.*, 2011) than younger individuals and therefore require less pathological tau to produce a similar level of cognitive impairment. Due to the combined effects of Alzheimer's disease and non-Alzheimer's disease pathological changes, older CI A+ individuals with extremely high levels of pathologic tau, on a par with that seen younger CI A+, are perhaps most often too impaired to participate in research studies.

Our final aim was to estimate sample sizes that would be needed to power two different types of clinical trials using change in tau PET, cortical volume, and memory/mental status indices as outcome measures (Table 2). The first scenario was a trial in CU A+ individuals. This would be analogous to the A4 (Antiamyloid Therapy for Asymptomatic Alzheimer's Disease) study (Sperling *et al.*, 2014), which enrols CU A+ individuals. The primary outcome is modification of the rate of cognitive decline; however, longitudinal tau PET is being acquired in a subset to test the hypothesis that an anti-amyloid intervention can modify the natural rate of pathological tau accumulation. Our data indicate that among the four tau PET meta-regions of interest, sample sizes are smallest with the temporal composite for the CU A+ group (however, this was not appreciably different from the sample sizes for the early Alzheimer's disease change meta-region of interest).

Table 3 Effect of partial volume correction

Parameter	CU A+			CI A+		
	Change/year Mean (SD)	Effect size (SE)[a]	*n*	Change/year Mean (SD)	Effect size (SE)[a]	*n*
Early AD meta-ROI						
PVC	0.013 (0.028)	0.45 (0.19)	1228	0.074 (0.104)	0.71 (0.16)	499
No PVC	0.011 (0.024)	0.46 (0.18)	1191	0.069 (0.104)	0.66 (0.16)	580
Late AD meta-ROI						
PVC	0.004 (0.025)	0.17 (0.18)	8805	0.077 (0.081)	0.95 (0.17)	282
No PVC	0.002 (0.024)	0.09 (0.18)	28548	0.054 (0.067)	0.81 (0.15)	383
Whole brain meta-ROI						
PVC	0.007 (0.025)	0.27 (0.18)	3513	0.053 (0.064)	0.83 (0.16)	364
No PVC	0.004 (0.020)	0.20 (0.19)	6464	0.040 (0.054)	0.73 (0.15)	476
Temporal meta-ROI						
PVC	0.012 (0.026)	0.48 (0.19)	1087	0.074 (0.082)	0.91 (0.18)	308
No PVC	0.009 (0.022)	0.42 (0.18)	1432	0.056 (0.071)	0.79 (0.17)	404

Sample size estimates per arm for a clinical trial targeting a 25% reduction in annual change in tau PET meta-regions of interest (SUVR per year) with 80% power and alpha = 0.05 within CU A+ and CI A+, separately for PVC and no PVC.

[a]Effect size is calculated as the mean divided by the standard deviation in the sample. The standard error of the effect size estimate is determined from 10 000 bootstrap replicates.

AD = Alzheimer's disease; ROI = region of interest.

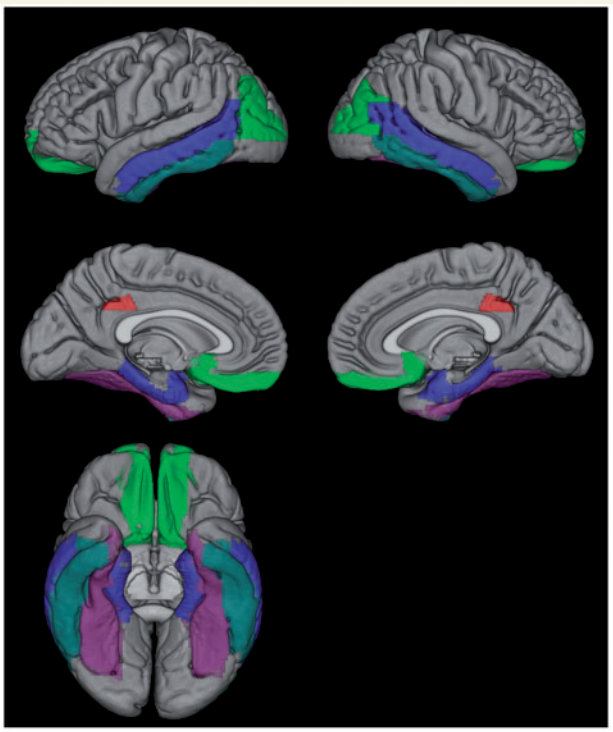

Figure 4 Topography of meta-regions of interest. The early Alzheimer's disease change meta-region of interest is indicated in red; the late Alzheimer's disease change meta-region of interest in green; and the temporal composite in blue. The inferior temporal region of interest appears aqua because it is part of both the late Alzheimer's disease change and temporal meta-regions of interest (overlap between blue and green). Similarly, the fusiform gyrus appears magenta because it is part of both the early Alzheimer's disease change and temporal meta-regions of interest (overlap between red and blue). The whole brain meta-region of interest is not illustrated.

This may seem counterintuitive given that the early Alzheimer's disease change meta-region of interest seemed to best separate the CU A+ from CU A– groups. The explanation is that while the early Alzheimer's disease and temporal meta-regions of interest had similar rates of increase, the variation across individuals was slightly greater in the early Alzheimer's disease change meta-region of interest. This is partly, or perhaps primarily, because the temporal composite measure included a greater number of voxels than the early Alzheimer's disease change meta-region of interest (Fig. 4) hence it may be a more precise measure. Pooling A+ MCI and dementia participants into a single CI A+ group is analogous to the recent PRIME trial (Sevigny *et al.*, 2016). The late Alzheimer's disease change meta-region of interest had the smallest sample size of the four meta-regions of interest among the CI A+ group. However, this was not appreciably different from the sample sizes for the whole brain or temporal meta-regions of interest. For both CU A+ and CI A+, the smallest sample sizes were obtained with the cortical volume rate measure (TBM-SyN), the largest with the memory/mental status measure, and sample sizes for the tau PET meta-region of interest (temporal in CU A+ and late Alzheimer's disease in CI A+) were in-between these two. It is worthwhile noting that sample sizes were similar with TBM-SyN and tau PET in CI A+, indicating that change in tau PET SUVR (Baker *et al.*, 2017) should be an effective outcome measure in trials of putative disease modifying agents.

Some individuals with negative slopes are seen in Figs 1–3. Figure 3 illustrates that this phenomenon is more common among those with low baseline values compared to those with high baseline values. While there is some suggestion that CSF phosphorylated tau values could decline late in the Alzheimer's disease continuum (Fagan *et al.*, 2014), we

interpret negative slopes in this tau PET data to represent measurement error. That is certainly the case for many individuals with low baseline values who are more likely than those with high baseline values to have no real change in tau. Individuals with no real (biological) change in tau are equally likely to have a small positive or negative slope centred around zero due to measurement error.

We did not estimate sample sizes among CU A− because rates of tau accumulation were very low in this group. The low natural rate of tau accumulation in CU individuals with normal amyloid levels suggests that tau PET would not likely be a good outcome measure of anti-tau interventions in this group even if preventing the appearance of tau deposition below the PET threshold of detection was an effective therapeutic strategy.

A strength of this study is that we measured within-person rates of tau PET change which directly support inferences about the progression of disease and accumulation of pathological 3R/4R fibrillar tau. In contrast, mechanistic inferences can only be supported indirectly with cross-sectional data. We recognize several weaknesses. Sample sizes were modest. We expect that greater group-wise differences in rates (e.g. between CU A+ and CU A−) might have been found with a larger sample. Our conclusions are based on group averages with short follow-up intervals whereas long-term within-person follow-up would be preferable. Due to the recent development of tau PET, availability of those data will require further maturation of research cohorts. It would have been desirable to take a more granular approach to defining earlier versus later changing measures by creating a greater number of group-wise contrasts. At this point though, we have too few CI A+ participants with longitudinal tau to effectively split that group into separate MCI and mild and moderate dementia A+ groups. This does not seem like a major shortcoming though as precedent exists for combining prodromal Alzheimer's disease and dementia into a single CI A+ group (Sevigny *et al.*, 2016).

We focused on comparing rate measurements across different locations in the brain but there are many other technical aspects that likely have a significant impact on longitudinal tau PET measures. One of these is the use of PVC, which we only briefly examined. In general, mean rates of change and variance were slightly greater with PVC than without but sample size estimates were generally smaller with PVC (Table 3). We recognize that many different approaches to PVC have been proposed (Shidahara *et al.*, 2017) and we briefly compared only one of these to no PVC. Therefore, whether or not PVC is recommended for serial tau PET measures and, if so, which of many possible approaches is optimal remains an open question. Other data processing steps such as smoothing, PET-MRI versus PET only methods, transformation of data to a common space (or not), and magnetic resonance segmentation methods will also likely impact longitudinal PET measures (Maass *et al.*, 2017). As was the case for amyloid PET (Chen *et al.*, 2015; Landau *et al.*, 2015; Schwarz *et al.*, 2017) choice of normalizing reference region in particular seems likely to have an important impact on longitudinal measurement precision (Southekal *et al.*, 2017). These possible technical variations remain an active area of investigation and it seems very likely that the precision of longitudinal tau PET measures will improve with advances in technical approaches. This in turn should result in greater effect sizes (smaller sample sizes) for tau PET as an outcome measure for clinical trials compared to those in Tables 2 and 3.

Acknowledgements

The authors would like to acknowledge the Alexander Family Alzheimer's Disease Research Professorship of the Mayo Clinic, the GHR Foundation, and the Elsie and Marvin Dekelboum Family Foundation. We would like to greatly thank AVID Radiopharmaceuticals, Inc., for their support in supplying AV-1451 precursor, chemistry production advice and oversight, and FDA regulatory cross-filing permission and documentation needed for this work. The authors report no relevant conflicts of interest.

Funding

The authors are supported by NIH R01 AG011378, R01 AG041851, U01 AG006786, R01 AG034676, R01 NS097495, and P50 AG016574.

Supplementary material

Supplementary material is available at *Brain* online.

References

Baker SL, Lockhart SN, Price JC, He M, Huesman RH, Schonhaut D, et al. Reference tissue-based kinetic evaluation of 18F-AV-1451 for Tau imaging. J Nucl Med 2017; 58: 332–8.

Bejanin A, Schonhaut DR, La Joie R, Kramer JH, Baker SL, O'Neil JP, et al. Do neurodegeneration or amyloid pathology contribute to the relationship between AV-1451 and cognitive symptoms in Alzhimer's disease? In: Johnson KA, Jagust WJ, Klunk WE, Mathis CA, editors. 11th Human Amyloid Imaging, Jan 11-13, 2017, Miami, Florida. p. 252. www.worldeventsforum.com/hai.

Braak H, Braak E. Neuropathological stageing of Alzheimer-related changes. Acta Neuropathol 1991; 82: 239–59.

Braak H, Braak E. Frequency of stages of Alzheimer-related lesions in different age categories. Neurobiol Aging 1997; 18: 351–7.

Brier MR, Gordon B, Friedrichsen K, McCarthy J, Stern A, Christensen J, et al. Tau and Aβ imaging, CSF measures, and cognition in Alzheimer's disease. Sci Transl Med 2016; 8: 338ra66.

Buckley RF, Hanseeuw B, Schultz AP, Vannini P, Aghjayan SL, Properzi MJ, et al. Region-specific association of subjective cognitive decline with tauopathy independent of global beta-amyloid burden. JAMA Neurol 2017; 74: 1455–63.

Chen K, Roontiva A, Thiyyagura P, Lee W, Liu X, Ayutyanont N, et al. Improved power for characterizing longitudinal amyloid-beta

PET changes and evaluating amyloid-modifying treatments with a cerebral white matter reference region. J Nucl Med 2015; 56: 560–6.
Chhatwal JP, Schultz AP, Marshall GA, Boot B, Gomez-Isla T, Dumurgier J, et al. Temporal T807 binding correlates with CSF tau and phospho-tau in normal elderly. Neurology 2016; 87: 920–6.
Chiotis K, Saint-Aubert L, Rodriguez-Vieitez E, Leuzy A, Almkvist O, Savitcheva I, et al. Longitudinal changes of tau PET imaging in relation to hypometabolism in prodromal and Alzheimer's disease dementia. Mol Psychiatry 2017, in press. [Epub ahead of print].
Cho H, Choi JY, Hwang MS, Kim YJ, Lee HM, Lee HS, et al. *In vivo* cortical spreading pattern of tau and amyloid in the Alzheimer disease spectrum. Ann Neurol 2016; 80: 247–58.
de Calignon A, Polydoro M, Suarez-Calvet M, William C, Adamowicz DH, Kopeikina KJ, et al. Propagation of tau pathology in a model of early Alzheimer's disease. Neuron 2012; 73: 685–97.
Fagan AM, Xiong C, Jasielec MS, Bateman RJ, Goate AM, Benzinger TL, et al. Longitudinal change in CSF biomarkers in autosomal-dominant Alzheimer's disease. Sci Transl Med 2014; 6: 226ra30.
Fox NC, Cousens S, Scahill R, Harvey RJ, Rossor MN. Using serial registered brain magnetic resonance imaging to measure disease progression in Alzheimer disease: power calculations and estimates of sample size to detect treatment effects. Arch Neurol 2000; 57: 339–44.
Gordon BA, Friedrichsen K, Brier M, Blazey T, Su Y, Christensen J, et al. The relationship between cerebrospinal fluid markers of Alzheimer pathology and positron emission tomography tau imaging. Brain 2016; 139 (Pt 8): 2249–60.
Hasite T, Tibshirani R, Friedman J. The elements of statistical learning. 2nd edn. New York: Springer-Verlag; 2009.
Jack CR Jr, Knopman DS, Jagust WJ, Petersen RC, Weiner MW, Aisen PS, et al. Tracking pathophysiological processes in Alzheimer's disease: an updated hypothetical model of dynamic biomarkers. Lancet Neurol 2013; 12: 207–16.
Jack CR Jr, Wiste HJ, Weigand SD, Therneau TM, Lowe VJ, Knopman DS, et al. Defining imaging biomarker cut points for brain aging and Alzheimer's disease. Alzheimers Dement 2017; 13: 205–16.
Johnson KA, Shultz A, Betensky RA, Becker JA, Sepulcre J, Rentz DM, et al. Tau positron emission tomographic imaging in aging and early Alzheimer's disease. Ann Neurol 2016; 79: 110–9.
Jones DT, Graff-Radford J, Lowe VJ, Wiste HJ, Gunter JL, Senjem ML, et al. Tau, amyloid, and cascading network failure across the Alzheimer's disease spectrum. Cortex 2017; 97: 143–59.
Klunk WE, Engler H, Nordberg A, Wang Y, Blomqvist G, Holt DP, et al. Imaging brain amyloid in Alzheimer's disease with Pittsburgh Compound-B. Ann Neurol 2004; 55: 306–19.
Klunk WE, Koeppe RA, Price JC, Benzinger T, Devous M, Jagust W, et al. The Centiloid Project: standardizing quantitative amyloid plaque estimation by PET. Alzheimers Dement 2015; 11: 1–15.e1–4.
Kokmen E, Smith GE, Petersen RC, Tangalos E, Ivnik RC. The short test of mental status. Correlations with standardized psychometric testing. Arch Neurol 1991; 48: 725–8.
Koychev I, Gunn RN, Firouzian A, Lawson J, Zamboni G, Ridha B, et al. PET Tau and amyloid-beta burden in mild Alzheimer's disease: divergent relationship with age, cognition, and cerebrospinal fluid biomarkers. J Alzheimers Dis 2017; 60: 283–93.
La Joie R, Bejanin A, Fagan AM, Ayakta N, Baker SL, Bourakova V, et al. Relationships between AV1451-PET and CSF biomarkers in a heterogeneous clinical sample. In: Johnson KA, Jagust WJ, Klunk WE, Mathis CA, editors. 11th Human Amyloid Imaging; 2017 Jan 11-13, 2017; Miami, Florida. p. 258. www.worldeventsforum.com/hai.
Landau SM, Fero A, Baker SL, Koeppe R, Mintun M, Chen K, et al. Measurement of longitudinal beta-amyloid change with 18F-florbetapir PET and standardized uptake value ratios. J Nucl Med 2015; 56: 567–74.
Liu L, Drouet V, Wu JW, Witter MP, Small SA, Clelland C, et al. Trans-synaptic spread of tau pathology *in vivo*. PLoS One 2012; 7: e31302.
Lowe VJ, Wiste HJ, Senjem ML, Weigand SD, Therneau TM, Boeve BF, et al. Widespread brain tau and its association with ageing, Braak stage and Alzheimer's dementia. Brain 2018; 141: 271–87.
Lowe V, Wiste H, Senjem M, Weigand S, Therneau TM, Boeve B, et al. Widespread brain Tau and its association with aging, braak stage, and Alzheimer's dementia. Brain 2018; 147: 271–87.
Maass A, Landau S, Baker SL, Horng A, Lockhart SN, La Joie R, et al. Comparison of multiple tau-PET measures as biomarkers in aging and Alzheimer's disease. Neuroimage 2017; 157: 448–63.
Markesbery WR, Schmitt FA, Kryscio RJ, Davis DG, Smith CD, Wekstein DR. Neuropathologic substrate of mild cognitive impairment. Arch Neurol 2006; 63: 38–46.
Marks SM, Lockhart SN, Baker SL, Jagust WJ. Tau and beta-amyloid are associated with medial temporal lobe structure, function, and memory encoding in normal aging. J Neurosci 2017; 37: 3192–201.
McKhann GM, Knopman DS, Chertkow H, Hyman BT, Jack CR Jr, Kawas CH, et al. The diagnosis of dementia due to Alzheimer's disease: recommendations from the National Institute on Aging and the Alzheimer's Assocation Workgroup. Alzheimers Dement 2011; 7: 263–9.
Meltzer CC, Leal JP, Mayberg HS, Wagner HN Jr, Frost JJ. Correction of PET data for partial volume effects in human cerebral cortex by MR imaging. J Comput Assist Tomogr 1990; 14: 561–70.
Mishra S, Gordon BA, Su Y, Christensen J, Friedrichsen K, Jackson K, et al. AV-1451 PET imaging of tau pathology in preclinical Alzheimer disease: defining a summary measure. Neuroimage 2017; 161: 171–8.
Nasrallah IM, Chen YJ, Hsieh MK, Philips JS, Ternes K, Stockbower G, et al. 18F-Flortaucipir PET-MRI correlations in non-amnestic and amnestic variants of Alzheimer disease. J Nucl Med 2018; 59: 299–306.
Nelson PT, Head E, Schmitt FA, Davis PR, Neltner JH, Jicha GA, et al. Alzheimer's disease is not "brain aging": neuropathological, genetic, and epidemiological human studies. Acta Neuropathol 2011; 121: 571–87.
Ossenkoppele R, Schonhaut DR, Scholl M, Lockhart SN, Ayakta N, Baker SL, et al. Tau PET patterns mirror clinical and neuroanatomical variability in Alzheimer's disease. Brain 2016; 139 (Pt 5): 1551–67.
Petersen RC. Mild cognitive impairment as a diagnostic entity. J Intern Med 2004; 256: 183–94.
Phillips JS, Das SR, McMillan CT, Irwin DJ, Roll EE, Da Re F, et al. Tau PET imaging predicts cognition in atypical variants of Alzheimer's disease. Hum Brain Mapp 2018; 39: 691–708.
Pontecorvo MJ, Devous MD, Sr., Navitsky M, Lu M, Salloway S, Schaerf FW, et al. Relationships between flortaucipir PET tau binding and amyloid burden, clinical diagnosis, age and cognition. Brain 2017; 140: 748–63.
Roberts RO, Geda YE, Knopman DS, Cha RH, Pankratz VS, Boeve BF, et al. The Mayo Clinic Study of Aging: design and sampling, participation, baseline measures and sample characteristics. Neuroepidemiology 2008; 30: 58–69.
Schneider JA, Arvanitakis Z, Leurgans SE, Bennett DA. The neuropathology of probable Alzheimer disease and mild cognitive impairment. Ann Neurol 2009; 66: 200–8.
Scholl M, Lockhart SN, Schonhaut DR, O'Neil JP, Janabi M, Ossenkoppele R, et al. PET Imaging of tau deposition in the aging human brain. Neuron 2016; 89: 971–82.
Scholl M, Ossenkoppele R, Strandberg O, Palmqvist S, Jogi J, Ohlsson T, et al. Distinct 18F-AV-1451 tau PET retention patterns in early- and late-onset Alzheimer's disease. Brain 2017; 140: 2286–94.
Schwarz AJ, Yu P, Miller BB, Shcherbinin S, Dickson J, Navitsky M, et al. Regional profiles of the candidate tau PET ligand 18F-AV-1451 recapitulate key features of Braak histopathological stages. Brain 2016; 139 (Pt 5): 1539–50.
Schwarz CG, Senjem ML, Gunter JL, Tosakulwong N, Weigand SD, Kemp BJ, et al. Optimizing PiB-PET SUVR change-over-time measurement by a large-scale analysis of longitudinal reliability, plausibility, separability, and correlation with MMSE. Neuroimage 2017; 144: 113–27.

Sepulcre J, Grothe MJ, Sabuncu M, Chhatwal J, Schultz AP, Hanseeuw B, et al. Hierarchical organization of Tau and amyloid deposits in the cerebral cortex. JAMA Neurol 2017; 74: 813–20.

Sevigny J, Chiao P, Bussiere T, Weinreb PH, Williams L, Maier M, et al. The antibody aducanumab reduces Abeta plaques in Alzheimer's disease. Nature 2016; 537: 50–6.

Shidahara M, Thomas BA, Okamura N, Ibaraki M, Matsubara K, Oyama S, et al. A comparison of five partial volume correction methods for Tau and Amyloid PET imaging with [18F]THK5351 and [11C]PIB. Ann Nucl Med 2017; 31: 563–9.

Sonnen JA, Santa Cruz K, Hemmy LS, Woltjer R, Leverenz JB, Montine KS, et al. Ecology of the aging human brain. Arch Neurol 2011; 68: 1049–56.

Southekal S, Devous MD Sr, Kennedy I, Navitsky M, Lu M, Joshi AD, et al. Flortaucipir F 18 quantitation using a parametric estimate of reference signal intensity (PERSI). J Nucl Med 2017, in press. [Epub ahead of print].

Sperling RA, Rentz DM, Johnson KA, Karlawish J, Donohue M, Salmon DP, et al. The A4 study: stopping AD before symptoms begin? Sci Transl Med 2014; 6: 228fs13.

Vemuri P, Senjem ML, Gunter JL, Lundt ES, Tosakulwong N, Weigand SD, et al. Accelerated vs. unaccelerated serial MRI based TBM-SyN measurements for clinical trials in Alzheimer's disease. Neuroimage 2015; 113: 61–9.

Villemagne VL, Fodero-Tavoletti MT, Masters CL, Rowe CC. Tau imaging: early progress and future directions. Lancet Neurol 2015; 14: 114–24.

Wang L, Benzinger TL, Su Y, Christensen J, Friedrichsen K, Aldea P, et al. Evaluation of Tau imaging in staging Alzheimer disease and revealing interactions between beta-amyloid and tauopathy. JAMA Neurol 2016; 73: 1070–7.

Xia C, Makaretz SJ, Caso C, McGinnis S, Gomperts SN, Sepulcre J, et al. Association of *in vivo* [18F]AV-1451 Tau PET imaging results with cortical atrophy and symptoms in typical and atypical Alzheimer disease. JAMA Neurol 2017; 74: 427–36.